Quantum Electronics **52** (5) 474–481 (2022)

QUANTUM DOTS

https://doi.org/10.1070/QEL18046

Interaction of an array of single-electron quantum dots with a microcavity field with allowance for Coulomb correlations

A.V. Tsukanov, I.Yu. Kateev

Abstract. **We consider an ordered array of semiconductor single-electron quantum dots located in the antinode of a mode of a microcavity based on a two-dimensional photonic crystal. The influence of Coulomb effects on the energy exchange between quantum dots and the mode is studied in arrays for different numbers of dots. The stability of resonant electron–photon dynamics is analysed as a function of technological deviations of the dot parameters caused by the imperfection of the manufacturing procedure. Using the data of numerical simulation of the spectroscopic response of the system, criteria are formulated for using such a structure as a detector of localised charges. The parameters of the photonic crystal are chosen, which make it possible to implement the proposed measurement scheme.**

Keywords: *quantum measurement, laser, photonic crystals, quantum dots, electrons, Coulomb interaction, Förster effect.*

1. Introduction

Multicomponent systems based on semiconductor quantum dots (QDs) are widely used in various micro- and nanoelectronic devices [1–3]. A high degree of discreteness of the energy spectrum promotes the use of QDs as functional elements of such devices as a single-electron transistor [4], quantum point contact [5], quantum turnstile [6], and cellular automaton [7]. There are a number of proposals on how to implement the concept of a quantum chip for processing and storing quantum information using QDs controlled by external fields. The most promising for practical application are schemes for encoding information into electronic, electron–hole (exciton) and spin degrees of QD freedom [8–10]. According to the method of external control, they can be divided into electrical, optical and magnetic. Currently, there are working prototypes of all the mentioned devices. The main advantages of QDs include their compactness, a variety of shapes and types, the ability to operate at relatively high temperatures, and reliable compatibility with other chip components. If we talk about quantum information processing, then the main problem is maintaining the coherence of the state of quantum bits (qubits), which requires maximum suppression of dissipative processes. In addition, it is necessary to be able to control the size, chemical composition and position of the QD in space, as well as to ensure that the control interface is placed in close proximity to the QD. All these issues are being actively studied.

A serious problem for theoretical modelling is the incomplete consideration of the Coulomb effects caused by the interaction of QD electrons. As a rule, researchers confine themselves to calculating the Stark shifts of the QD energy levels. This approach is sufficient only for the conceptual analysis of elementary quantum operations [11, 12]. The point charge approximation can be used to qualitatively estimate the shift energy as a function of the distance between the centres of two QDs. At the same time, there are a number of problems in which it is required not only to correctly calculate the diagonal matrix elements (i.e., Stark shifts) of the Coulomb interaction Hamiltonian for a given spatial distribution of the electron density in a QD, but also to take into account off-diagonal matrix elements with the required accuracy. The latter describe two-particle processes that manifest themselves in the modulation of the time dependences of the probability amplitudes of the QD states.

The aim of this work is to study the features of the spectral response of an array of single-electron QDs placed in the mode of a high-Q microcavity (MC) based on a two-dimensional photonic crystal (PC). Calculating the coefficient of photon transmission through the MC makes it possible to determine the operating characteristics of the structure and formulate criteria for its being in one or another dynamic mode. As follows from the simulation results, the Coulomb effects can either increase or decrease the sensitivity of the array to changes in the ambient field produced by an electron in an external (measured) QD, depending on the parameters of the QD array and MC. In addition, the stability of the system response to fluctuations in the QD parameters caused by the imperfection of their manufacturing technology was studied. Critical deviations are indicated, above which the enhancement of the electron–photon interaction becomes ineffective. Using the numerical solution of the Maxwell equations by the finite-difference time-domain method, the optical characteristics of PCs with defects of various types are simulated. The PC parameters are found that ensure the equality of all Rabi frequencies of the MC mode energy exchange with each QD in an array consisting of a large number of QDs.

2. Spectroscopic response of an array of single-electron QDs interacting with the MC mode

To describe the quantum evolution of an array of N single-electron QDs located inside the optical volume of the MC mode with a frequency ω_c, we use the following model. Let there be two states in the kth QD: the ground state $|g_k\rangle$ with

A.V. Tsukanov, I.Yu. Kateev Valiev Institute of Physics and Technology, Russian Academy of Sciences, Nakhimovskii prosp. 34, 117218 Moscow, Russia; e-mail: ikateyev@mail.ru

Received 13 October 2021; revision received 19 February 2022
Kvantovaya Elektronika **52** (5) 474–481 (2022)
Translated by V.L. Derbov

energy $\varepsilon_{g,k}$ and the excited state $|e_k\rangle$ with energy $\varepsilon_{e,k}$ (we do not consider its other states). The frequencies of optical electronic transitions are assumed the same for all QDs: $\omega_k = \varepsilon_{e,k} - \varepsilon_{g,k} = \omega_a$ (hereinafter, $\hbar \equiv 1$). The Rabi frequency of the energy exchange of the kth QD with the MC mode because of photon emission/absorption is $\Omega_k = \langle g_k| -e\boldsymbol{E}_c\boldsymbol{r}_k|e_k\rangle$, where $\boldsymbol{E}_c$ is the amplitude of the MC mode field; and $\boldsymbol{r}_k$ is the electron radius vector in the QD. The amplitude of the mode field depends both on the geometry of the QD and on its spatial position in the volume of the mode, and can differ significantly even for neighbouring QDs. As already mentioned above, the Coulomb effects play an important role in the dynamics of a many-electron system. They can be divided into diagonal and off-diagonal effects. The first group is associated with energy shifts of QD states caused by the interaction of electrons. The second group describes: a) resonant processes that cause energy transfer between two QDs without charge transfer (Förster effect) [13]; and b) non-energy-conserving virtual processes that lead to dynamic shifts in the QD levels. The general expression for the Coulomb matrix elements is given by the formula [14]

$$V_{k,m} = 2\int\int \mathrm{d}\boldsymbol{r}_k \mathrm{d}\boldsymbol{r}_m \Psi_{\mathrm{f}}^*(\boldsymbol{r}_k)\Psi_{\mathrm{f}}^*(\boldsymbol{r}_m)\Psi_{\mathrm{i}}(\boldsymbol{r}_m)\,\Psi_{\mathrm{i}}(\boldsymbol{r}_k)/|\boldsymbol{r}_k - \boldsymbol{r}_m|, \quad (1)$$

where $\Psi_{\mathrm{i(f)}}(\boldsymbol{r}_k)$ is the one-electron wave function of the initial (final) state, localised in the kth QD. For ease of identification, we supplement this notation with a superscript that specifies the specific process described by this matrix element. The units of measurement are effective atomic units: 1 e.a.u. = $\mathrm{Ry}^* = m^*\mathrm{Ry}/m_\mathrm{e}\varepsilon^2$ for energy and 1 e.a.u. = $a_\mathrm{B}^* = a_\mathrm{B}\mathrm{B}m_\mathrm{e}\varepsilon/m^*$ for the length, where Ry =13.6 eV is the Rydberg energy; $a_\mathrm{B} = 0.52\times10^{-10}$ m is the Bohr radius; m_e is the mass of a free electron; m^* is the effective electron mass; and ε is the permittivity of the semiconductor. For gallium arsenide GaAs (ε = 12, $m^* = 0.067$), we have $\mathrm{Ry}^* = 6$ meV and $a_\mathrm{B}^* = 10$ nm.

The parameters of the QD potentials are chosen such that the tunnel connection between neighbouring QDs can be ignored. This is achieved mainly due to the localisation of the energy levels of both the ground and excited states, as well as the positioning of neighbouring QDs at a distance significantly exceeding their characteristic size. Laser radiation with a frequency ω_las close to the frequency ω_c of the MC mode is focused on the sample surface. The energy is supplied to the MC mode from the laser field with the rate Ω_las. We will assume that the pump rate is such that no more than one excitation quantum can be present in the structure. Then the Hamiltonian of the system has the form:

$$\begin{aligned} H = {} & \omega_c a^\dagger a + \sum_{k=1}^{N}\omega_k |e_k\rangle\langle e_k| + \sum_{k>m} V_{k,m}^{\mathrm{gg}} |g_k g_m\rangle\langle g_k g_m| \\ & + \sum_{k\neq m} V_{k,m}^{\mathrm{ge}} |g_k e_m\rangle\langle g_k e_m| + \sum_{k\neq m} V_{k,m}^{\mathrm{ge,g}} |g_k g_m\rangle\langle e_k g_m| \\ & + \sum_{k\neq m} V_{k,m}^{\mathrm{ge,g}} |e_k g_m\rangle\langle g_k g_m| + \sum_{k>m} V_{k,m}^{\mathrm{F}} |g_k e_m\rangle\langle g_m e_k| \\ & + \sum_{k>m} V_{k,m}^{\mathrm{F}} |e_k g_m\rangle\langle e_m g_k| - \sum_{k=1}^{N}\Omega_k(|e_k\rangle\langle g_k|a + |g_k\rangle\langle e_k|a^\dagger) \\ & + 2\Omega_\mathrm{las}\cos(\omega_\mathrm{las}t)(a^\dagger + a). \end{aligned} \quad (2)$$

Here a is the photon annihilation operator in the MC mode; when describing the energy exchange between QD and the mode, the rotating wave approximation is used, which assumes that the condition $\omega_k \gg \Omega_k$ is satisfied. The Förster energies $V_{k,m}^\mathrm{F}$ characterise the frequency of the resonant energy exchange between QDs caused by the Coulomb interaction. This process is superimposed on the electron–photon dynamics of the QD array in the MC, leading to its modification. Nonresonant Coulomb matrix elements $V_{k,m}^{\mathrm{ge,g}}$ generate small, rapidly oscillating dispersion shifts of the QD frequency.

Considering the configurations of QD arrays, one should choose those for which the majority of QDs will be located in the antinodes of the MC mode. The spatial dependence of the field amplitude is largely determined by the type and shape of the MC itself. In our work, we study a linear array (chain) of QDs located in the region of a defect in a lattice of Bragg holes of a two-dimensional photonic crystal forming a MC [15] (Fig. 1). The distance between the centres of neighbouring QDs is a_d. The dimension of the space of basis vectors is $N + 2$. The vector $|1\rangle = |g_k ... g_N\rangle|0_c\rangle$ describes the vacuum state of the electron–photon system, and the vector $|2\rangle = |g_k ... g_N\rangle|1_c\rangle$ corresponds to the presence of one photon in the MC mode. The remaining vectors $|k+2\rangle = |g_1 ... e_k ... g_N\rangle|0_c\rangle$ ($k = 1 - N$) describe the excitation of an electron in the kth QD. The state vector

$$|\Psi\rangle = \sum_{k=1}^{N+2} c_k |k\rangle$$

of the system is presented as an expansion in basis vectors with the coefficients c_k depending on time. The evolution of the state vector obeys the Schrödinger equation $\mathrm{i}\partial_t|\Psi\rangle = H|\Psi\rangle$ with the initial condition $|\Psi(0)\rangle = |1\rangle$. By applying the transformation

$$T = \exp\left[-\mathrm{i}\omega_\mathrm{las}t\left(a^\dagger a + \sum_{k=1}^{N}|e_k\rangle\langle e_k|\right)\right]$$

to the Hamiltonian H, its time dependence can be eliminated. In this case, the frequencies of the MC and QD modes are shifted by the frequency ω_las. In addition, one should take into account incoherent processes of photon dissipation associated with the escape of energy from the MC to the continuum at a rate of κ, and electronic relaxation at a rate of γ_k due

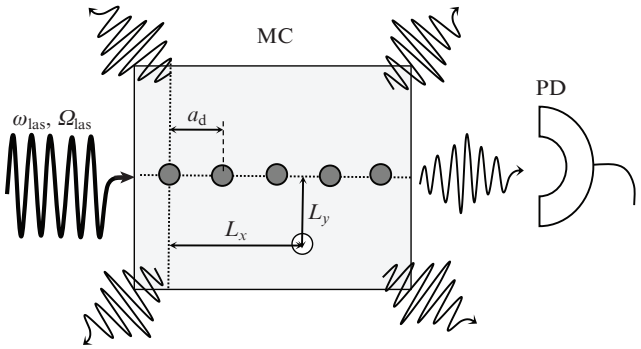

Figure 1. Schematic of a linear QD array placed in the antinode of the mode of an MC formed by a defect in a two-dimensional photonic crystal. A cw laser with a frequency ω_las performs pumping in a subphoton stationary regime at a rate Ω_las. The average number of photons emitted by the MC is measured by the photodetector PD. The tested QD with coordinates L_x and L_y is in the plane of the array.

to the interaction of the kth QD with the phonon environment. A rigorous consideration of these phenomena is possible within the formalism of the density matrix and the Lindblad equation; however, an approximate solution that is valid for a low probability of excitation of the system from a vacuum state can be found using a simpler formalism of the Schrödinger equation. To this end, in Eqn (2) one should make the replacement $\omega_c \to \omega_c - i\kappa$ and $\omega_k \to \omega_k - i\gamma_k$.

Let us choose the value

$$\varepsilon_0 = \sum_{k=1}^{N} \varepsilon_{g,k} + \sum_{m>k} V_{km}^{gg}$$

as the origin of the 'QD array +MC' system energy. In addition, we assume that the energies of the off-diagonal Coulomb components $V_{k,m}^{ge,g}$ and $V_{k,m}^{F}$ can be ignored (see below). The Schrödinger equation, taking into account the above transformations and assumptions, turns out to be equivalent to the system of equations for the probability amplitudes of the basis vectors in the expansion of the state vector $|\Psi\rangle$

$$i\partial_t \begin{pmatrix} c_1 \\ c_2 \\ c_3 \\ \dots \\ c_N \end{pmatrix} = \begin{pmatrix} 0 & \Omega_{las} & 0 & \dots & 0 \\ \Omega_{las} & \delta_c - i\kappa & -\Omega_1 & \dots & -\Omega_N \\ 0 & -\Omega_1 & \delta_1 + G_1 - i\gamma_1 & \dots & 0 \\ \dots & \dots & \dots & \dots & \dots \\ 0 & -\Omega_N & 0 & \dots & \delta_N + G_N - i\gamma_N \end{pmatrix} \begin{pmatrix} c_1 \\ c_2 \\ c_3 \\ \dots \\ c_N \end{pmatrix}, \quad (3)$$

where the detuning $\delta_c = \omega_c - \omega_{las}$ of the mode frequency and the detunings $\delta_k = \omega_k - \omega_{las}$ of the QD transition frequencies from the laser frequency are defined and the parameters

$$G_k = \sum_{m \neq k} (V_{km}^{ge} - V_{km}^{gg})$$

are introduced to characterise the nonequivalence of the Coulomb interaction of an electron in the ground state of the kth QD with electrons of the QD array in the vacuum and singly excited states. They represent frequency shifts of optical transitions in a QD.

Let us obtain an approximate solution of system (3) in the steady state of subphoton pumping, when $c_1 \approx 1$ and $\partial_t c_k \approx 0$. We will be interested in the average photon population $\langle n \rangle = |c_2|^2$ of the MC mode, which determines the transmission coefficient, i.e. the number of photons coming from the source to the detector through the structure. A system of $N + 2$ homogeneous differential equations reduces to an inhomogeneous algebraic system of $N + 1$ equations, solving which we find an expression for the population of the MC mode:

$$\langle n \rangle \approx \frac{\Omega_{las}^2 F^2}{\left| (\delta_c - i\kappa) F - \sum_{m=1}^{N} \Omega_m^2 F_m \right|^2}, \quad (4)$$

where

$$F_m = \prod_{k \neq m}^{N} (\delta_k + G_k - i\gamma_k) \text{ and } F = \prod_{k=1}^{N} (\delta_k + G_k - i\gamma_k)$$

are products of resonant denominators of the QD array. In the absence of interaction between QDs and the MC mode ($\Omega_m = 0$), the denominator of expression (4) describes a Lorentz curve with a maximum at the frequency of the MC mode. In addition to the photon response of the structure itself, we will be interested in the effect of an additional (optically inactive) QD located outside the structure on its response. If there is an electron in a given QD, then this fact is manifested in additional shifts of transition frequencies in all QDs of the array, $G_k \to G_k + G_k'$. Therefore, by comparing the system response $\langle n \rangle$ with the calibration dependence $\langle n_0 \rangle$ obtained in the absence of an electron in the measured QD ($G_k' = 0$), one can determine whether the given QD contains an electron or not. The measurement is best carried out at the laser frequency for which the response difference is maximum. In order to characterise the sensitivity of the structure to external charges and fields quantitatively, we introduce a new function – the measurement contrast

$$S_{max} = \max\left(\frac{\langle n \rangle - \langle n_0 \rangle}{\langle n_0 \rangle} \right). \quad (5)$$

S_{max} depends both on the properties of the QD array and MC and on the distance to the tested QD. It is logical to assume that for an array consisting of a large number of QDs, the Coulomb interaction between it and the measured QD will substantially modify the response. However, as we will see in Section 4, this issue is much deeper and requires more careful study. In particular, the electron – electron interaction within the QD array itself has a significant impact on the measurement accuracy. In addition, there is a condition necessary for the collective Tavis – Cummings polariton splitting [16]. The issue is the approximate equality of the interaction coefficients of the array QDs and the MC mode: $\Omega_1 \approx \Omega_2 \approx \dots \approx \Omega_N \equiv \Omega_c$. If all QDs are oriented with respect to the Cartesian axes in the same way and have close parameters, then the second condition also requires that the mode field amplitude be constant in the region where QD is located. Section 3 shows examples of the MC where this condition is met.

3. Optimisation of the interaction between the QD array and the PC-based MC mode

There are several classes of high-Q semiconductor MCs, into which single QDs or their ensembles can be integrated using modern technologies. These are MCs that support whispering gallery modes, for example, microdisks [17], and Bragg resonators based on semiconductor layered heterostructures [18], and MCs, which are defects in the periodic lattice of one- and two-dimensional PCs [19, 20]. The last class of MCs is the most common due to the variety of types of defects determined by the location and number of missed holes, which allows different configurations of electromagnetic fields concentrated in a MC to be obtained. Let us list some of them: S1 is one missing hole in a square lattice [21], L3 is three missing holes arranged in a line [22], and H1 is one missing hole in a hexagonal lattice [23]. In one-dimensional PCs, on the contrary, there are limitations on the design of defects due to its linear structure, and the control of the electromagnetic field distribution in microdisks, e.g., by creating a shape asymmetry, can cause a decrease in their quality factor [24].

In this regard, we chose the MC in the form of a two-dimensional PC, in the centre of which there is a defective region ensuring the localisation of the electromagnetic field. As will be shown below, the operation of the detector is most

efficient when the eigenfrequency ω_c of the mode is close to the frequency ω_a of the electronic transition between the ground and excited states in the conduction band. Its typical value for GaAs QD is 0.1 eV, which corresponds to the photon wavelength in vacuum $\lambda_0 \approx 12$ μm. In addition, Section 4 shows the results for a linear array of a small number of QDs ($N = 6$), as well as for an extended chain of QDs ($N = 30$), with different distances between neighbouring QDs. In order for the Rabi frequency Ω_c in the array to be approximately the same for all QDs, it is necessary to select the PC parameters so that the electric field of one of its modes varies slightly over an array length of 0.3–2.5 μm. To this end, we simulated the spectral characteristics of a PC formed by a square array of holes etched in a GaAs plate with a period $b = 3$ μm and a radius $R = 0.37b$ (Fig. 2).

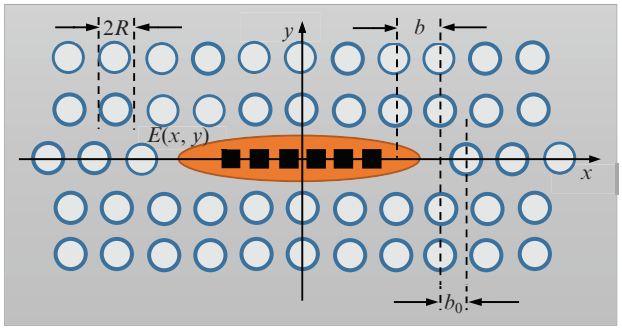

Figure 2. (Colour online) PC structure with an L5 defect with a variable size of the defective region (R is the hole radius, b is the lattice period, and b_0 is the shift of the central row of holes along the x axis with respect to the defective region). The array QD is located at the antinode of the electric field.

Calculation of eigenfrequencies and distribution of the electromagnetic field of the optical structure was carried out using the numerical solution of Maxwell's equations by the finite-difference time-domain method. First, we studied the optical properties of a PC, in the centre of which there is a defect representing a single missing hole (S1 defect). It supports two TE eigenmodes ($E_z = 0$) with wavelengths $\lambda_{c1} = 11.52$ μm and $\lambda_{c2} = 12.25$ μm. At a plate thickness of 10 μm, the maximum value E_0 of the single-photon electric field in the antinode exceeds 10 V cm^{-1} for both modes. Therefore, the Rabi frequency Ω_c of the energy exchange between an individual QD formed in the mode antinode region and MC will exceed 10^{-5} eV. As shown below, this is sufficient for the influence of the unwanted photon escape process, which leads to a decrease in the measurement contrast, to be small. However, for the first mode, the electric field reaches its maximum value far from the PC centre, near the holes surrounding the defective region, where the formation of QD is difficult. The array of QDs located in the central region of the PC will efficiently interact with the λ_{c2} mode, since its electric field has a maximum of $E_0 \approx 13$ V cm^{-1} directly at the centre of the defect (Fig. 3a).

Now let us estimate the linear size $d_{x(y)}$ of the electric field antinode, defining it as the size of the region along the $x(y)$ axis, at the boundaries of which the field decreases by half compared to the maximum value. It turned out that for this mode $d_x = 1.2$ μm and $d_y = 3.2$ μm. This means that for a PC with the above parameters, the Rabi frequency Ω_c will be

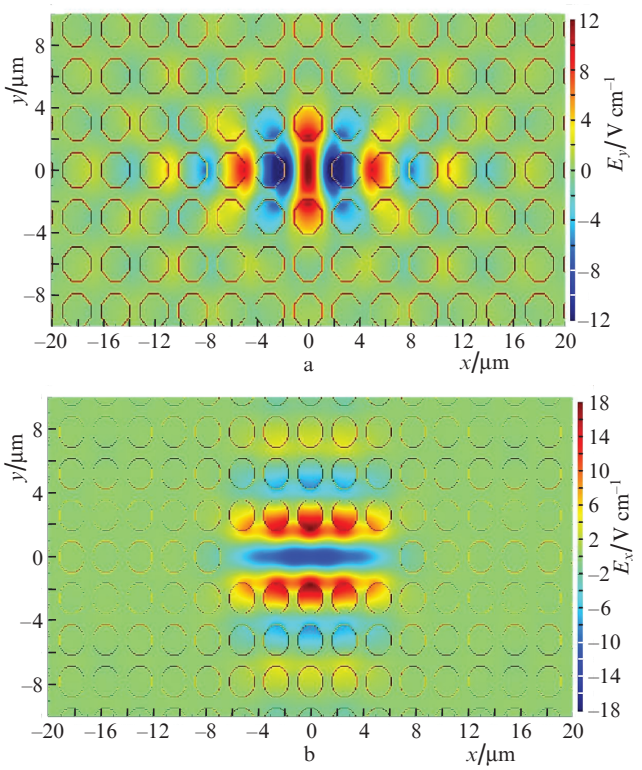

Figure 3. (Colour online) Two-dimensional distributions of (a) $E_y(x, y)$ for a PC with an S1 defect for the TE mode with a wavelength of 12.25 μm and (b) $E_x(x, y)$ for a PC with an L5 defect for the TE mode with a wavelength of 11.62 μm.

approximately the same for each QD in a linear array with a small number of points, $N \sim 5$, and its orientation relative to the PC axes can be arbitrary.

For large arrays ($N \sim 30$), in order to ensure the same value of Ω_c for all QDs, it is necessary to increase the size of the antinode region by selecting a PC of the corresponding geometry. We calculated the PC spectrum with a lattice period $b = 2.6$ μm, the defective region of which is formed by the absence of five holes along the x axis (L5 defect). The wavelength of one of the TE modes for PC with such a defect is $\lambda_c = 11.62$ μm, i.e., close to λ_0. The electric field of the mode has an extremum at the PC centre with a maximum value of $E_0 \approx 14$ V cm^{-1} and is elongated in the x axis direction; in this case, d_x reaches 10 μm (Fig. 3b). The vertical size of the mode antinode is about 1.1 μm. Therefore, by orienting horizontally an array of $N \sim 15$ QDs placed at the antinode, one can achieve almost the same value of Ω_c for each element. Thus, a PC with an L5 defect allows using both small linear arrays and arrays of a large number of QDs for detection, in contrast to a similar PC with an S1 defect considered above.

How to 'stretch' the electric field at the antinodes if it is necessary to use a QD array with an even greater number of elements? One of the ways is to increase the horizontal size of the defective area by shifting along the x axis the central row of holes, located to the left and right of the defective area, by some value b_0 (see Fig. 2). The value $b_0 = b = 2.6$ μm corresponds to a PC with an L7 defect, and the choice of $b_0 = 2b = 5.2$ μm makes it possible to obtain a PC structure with nine missing holes in the lattice. But how much will the eigenfrequency of the mode and the maximum value E_0 of the electric field at the antinode change under such a transformation? To answer these questions, we calculated the

spectrum and distribution of the electromagnetic field in a PC with an L5 defect for various values of b_0. It turned out that, on the one hand, an increase in b_0 in the range of 0–5.2 μm leads to an increase in d_x from 10 to 16 μm, as expected (Fig. 4). In this case, the mode wavelength increases insignificantly, up to 11.69 μm, i.e., by only 0.6%. Thus, at $b_0 \approx 5$ μm, the value of Ω_c for each QD in an array with $N = 30$ will be approximately the same, and all dots are tuned to resonance with the PC mode. The negative effect of an increase in the size of the defective region is a decrease in E_0, and hence Ω_c, by a factor of 1.3. This effect is shown below to enhance the influence of technological errors in the QD manufacturing and, as a result, to a decrease in the measurement contrast of the device.

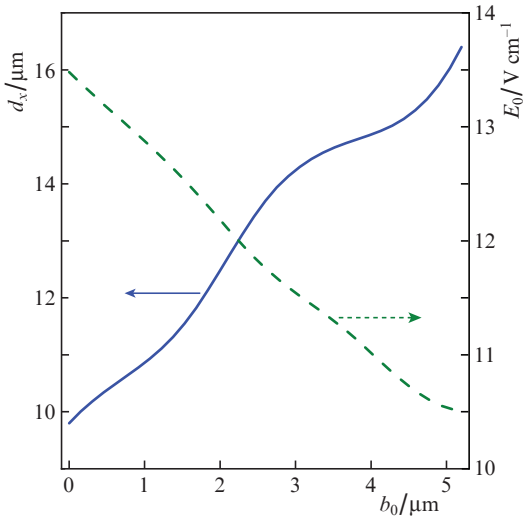

Figure 4. (Colour online) Dependences of the linear size d_x of the antinode region of the mode and the maximum value E_0 of the electric field in it on the value of b_0 for a PC with an L5 defect.

4. Dependence of the coefficient of photon transmission through the MC on the QD array parameters and the position of the measured QD

Let us consider a linear chain of one-electron QDs synthesised in the antinodes of the MC mode field. To calculate the Coulomb energies (1), we used the approximation of a three-dimensional rectangular well with infinitely high walls for the QD potential: $U(\mathbf{r}) = 0$ if $|x| \leqslant a_x/2$, $|y| \leqslant a_y/2$, $|z| \leqslant a_z/2$ and $U(\mathbf{r}) = \infty$ otherwise. To eliminate the influence of the Förster effect on the photon transfer through the MC, we choose an array structure for which this interaction is compensated. This can be achieved if each pair of neighbouring QDs of the array has orthogonal p-orbitals [14]. By alternating QDs with p_x- and p_y-orbitals, one can significantly weaken the Förster energy transfer between QDs and consider only the diagonal components of Hamiltonian (2). Figures 5 and 6 show the spectra of MCs containing a linear chain of $N = 10$ and 30 identical QDs with the above orbital configuration, as well as the QD frequency shifts, for compact ($a_d = 4$) and sparse ($a_d = 8$) chains.

Calculations of the matrix elements (1) of the Coulomb interaction of QDs included in Hamiltonian (2) showed that the frequency shifts of the one-electron QD depend as

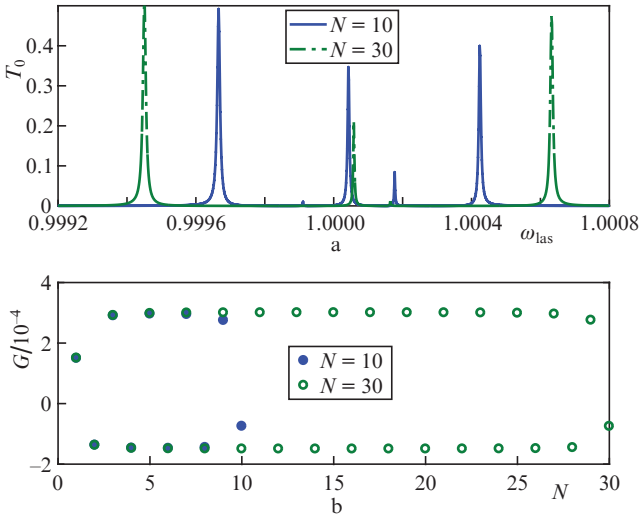

Figure 5. (Colour online) Spectroscopic characteristics of a hybrid structure based on a single-mode MC and a linear array of 10 and 30 QDs for a compact chain ($a_d = 4$). (a) The coefficient of laser photons transmission through the MC and (b) the dependence of the Coulomb shift of the electronic transition frequency in QD on its position in the chain. Positive (negative) shifts correspond to the orientation of the QD p-orbital along (across) the chain axis.

$G \sim a_p^2/L^3$ on the distance L between the centres of neighbouring QDs and on the effective radius a_p of the excited orbital. If $G \geqslant \Omega_c$, then the MC photon spectrum differs significantly from the MC spectrum obtained without considering the interaction between QDs due to the presence of additional resonances in the interval between the two extreme Tavis – Cummings (TC) polariton peaks. This testifies to the transformation of the electron–photon eigenstates of the structure, which is due to the shift asymmetry and leads to the appearance of 'light' components in some 'dark' states of the canonical TC model. If the condition $G \ll \Omega_c$ is satisfied, then the influence of the Coulomb effects is insignificant, and the spectrum is a Tavis – Cummings doublet. As the number N of QDs increases, there is a tendency to restore the doublet structure, accompanied by the suppression of 'Coulomb' resonances

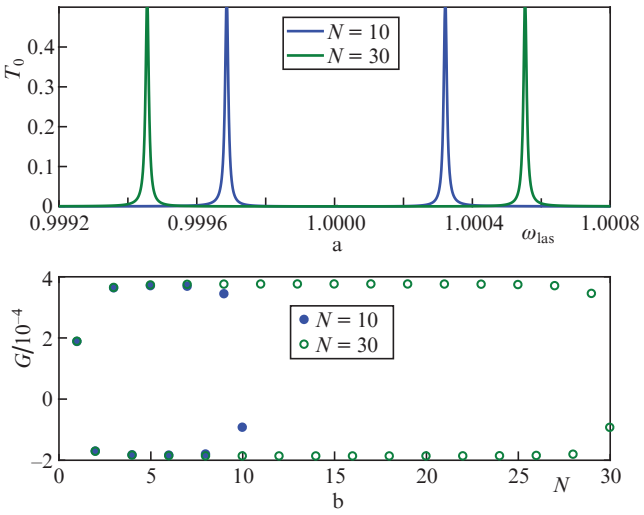

Figure 6. (Colour online) Spectroscopic characteristics of a hybrid structure based on a single-mode MC and a linear array of 10 and 30 QD for a sparse chain ($a_d = 8$). The notations are the same as in Fig.5.

in the central part of the spectrum. In addition, there is an increase by $\sqrt{N}$ times, already known to us, in the interaction energy of the QD array and the MC mode (splitting of polariton peaks). The first of these features is due to the enhancement of the interaction between the electron and photon subsystems with increasing N. Despite the smallness of the Rabi frequency Ω_c of an individual QD compared to the Coulomb shift of its frequency, the collective Rabi frequency increases and, for $N \geqslant (G/\Omega_c)^2$, overlaps the detunings associated with the shifts.

Compensation for the Coulomb QD frequency detunings, as well as the Förster energy, can be implemented by an appropriate choice of the QD parameters. In this case, the issue is choosing the QD potential depth, which would ensure the resonance of its electron frequency and the frequency of the MC mode, taking the electron–electron interaction in the chain into account. This adjustment can be implemented by varying the chemical composition/geometry of the QD at the stage of fabrication of the structure or by superimposing the local fields of metal gate electrodes located near the QD.

How will this modification of the spectrum of the structure affect its measuring properties? To answer this question, it is necessary to plot the dependences of the maximum contrast $S_{\max}$ (5) for structures with and without compensation for Coulomb shifts. Figure 7 shows the $S_{\max}$ for the QD chain interacting with the measured QD, which is located at a distance of $L_y = 4$ e.a.u. from its axis as a function of the longitudinal coordinate L_x. When varying the position of the QD centre along the chain, the contrast demonstrates broad peaks when the distance between the measured QD and the QDs of the chain with the p-orbital oriented along the y axis (in our case, QDs with even numbers) is minimal. If the shifts are compensated, then the number of peaks in this dependence increases, and the set of $S_{\max}$ maxima reflects the convergence of the measured QD with each QD of the chain. However, their values turn out to be less than without compensation. Thus, for high-precision electron detection, it is recommended to place the measured QD opposite those QDs of the chain, whose p-orbitals are oriented towards its centre, undertaking no shift compensation.

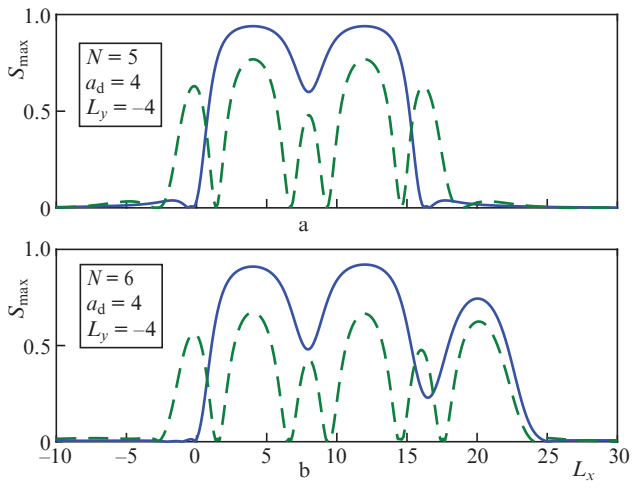

Figure 7. (Colour online) Dependences of the maximum value of the measurement contrast on the position of the tested QD along the chain with compensation ($G = 0$, solid curves) and without compensation ($G \neq 0$, dashed curves) of the Coulomb frequency shifts of the QD chain at $N =$ (a) 5 and (b) 6.

Let us study the behaviour of the function $S_{\max}$ depending on the distance L_y to the measured QD, as well as on the chain period a_d. As can be seen from Fig. 8, with increasing L_y, the expected decrease in contrast is accompanied by smoothing of the peaks. An increase in the distance between QDs weakens the electron–electron interaction within the chain, which is equivalent to compensation for shifts. This explains the similarity of the dependences in Fig. 7 at $G = 0$ and in Fig. 8. On the other hand, for a sparser chain, the contrast decreases faster as the measured QD moves away from it. Therefore, the Coulomb energy is an important resource, especially when measuring at a large distance to the object.

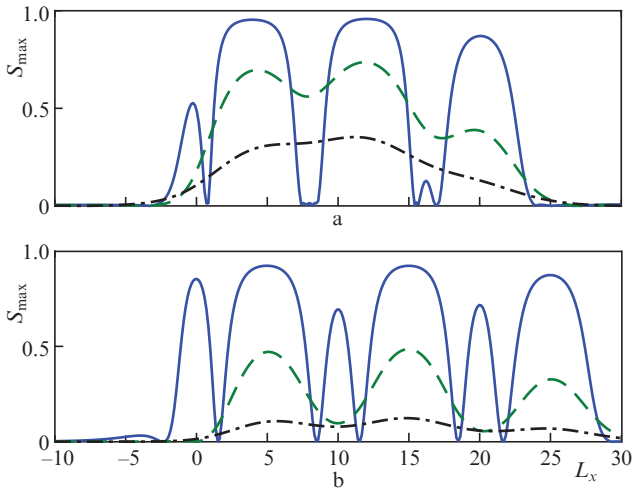

Figure 8. (Colour online) Dependences of the maximum value of the measurement contrast on the position of the tested QD along the chain for three distances from its centre to the axis of the chain [$L_y = 3$ (solid curves), 6 (dashed curves) and 9 (dash-dotted line)]; $N = 6$, and $a_d =$ (a) 4 and (b) 5.

In the course of comparing the spectroscopic dependences for the transmission coefficients through MC with QD chains of different lengths, we have already found out that an increase in the parameter N leads to an increase in the photon component against the background of the electronic subsystem and to restoration of the response shape without Coulomb interaction. The same effect also manifests itself when the measured QD is added, which does not significantly affect the spectrum of the system at $N \gg 1$.

An increase in the distance between the QD and the chain, as well as the distance between neighbouring QDs of the chain, manifests itself in a faster decrease in contrast (Fig. 9). In this case, the measurement efficiency remains relatively high only for a QD located at a distance $L_y = 4$. Thus, it is to be concluded that it is unsuitable to use extended linear chains of identical QDs in an MC for detecting an electron in an external QD at a large distance from this structure. Does it make sense then to talk about the prospects for using QD arrays? Recall that the original goal of increasing the number of optically active objects inside the MC that respond to external electric fields was to suppress dissipative effects associated with the uncontrolled escape of photons from the MC. In order to suppress this undesirable process, the condition $\Omega_c \sqrt{N} \geqslant \kappa$ must be satisfied. In this case, the total electron relaxation rate $N\gamma$ should also be less than this parameter. In our calculations, we assumed a stronger condition, $\Omega_c \gg \kappa$, to be satisfied, and therefore the peaks in Figs 5 and 6 are well

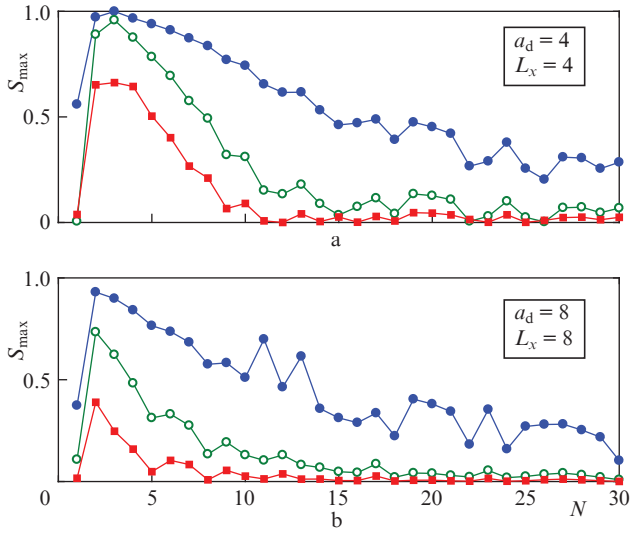

Figure 9. (Colour online) Dependences of the maximum value of the measurement contrast on the number of QD in the linear chain for several positions of the measured QD [L_y = (●) 4, (○) 6 and (■) 8] in the case of (a) compact and (b) sparse chains.

distinguishable even at a small number of QDs. For the opposite case ($\Omega_c \leqslant \kappa$), as N increases, the distinguishability of the peaks remains even at a low quality factor of the MC.

Having found out that the choice of N is of great importance, let us return to the study of the influence of other parameters of the QD chain on the measurement contrast. The data presented in Figs 7, 8 and 9 indicate the dependence of the function S_{max} on the distance between the QDs and on the frequency detuning between the QD and the MC mode. Due to the imperfection of the manufacturing technology of our structure, these values will have some random spread, described by a normal distribution with some standard deviation σ. Let us assume that the measured QD is located opposite the QD chain with an excited orbital oriented along the y axis. This configuration corresponds to the maximum contrast value. The transition frequency in a QD is the most important parameter that determines the degree of hybridisation of the electronic and photonic subsystems, and hence the very possibility of using photons to obtain information about the QD electronic state. If it turns out to be detuned from the frequency of the MC mode by a value greater than the interaction energy, then such a QD becomes 'dark' and ceases to affect photon transport.

The relationship between Ω_c and σ_ω determines the effect of QD frequency fluctuations on the degree of hybridisation of the photonic and electronic subsystems, and hence on the measurement accuracy. Even at $\sigma_\omega \approx 0.1\Omega_c$, the contrast drops by almost a factor of three compared to the structure of identical QDs (Fig. 10) that are in exact resonance with the MC mode. However, an increase in the interaction energy makes it possible to compensate for this undesirable effect. Another type of deviation is related to the inaccuracy of QD positioning in the chain, which again leads to uncontrolled Coulomb shifts of their frequencies. Obviously, the main source of error is the frequency shifts of those QDs that are closest to the measured QD. This means that its influence as a whole does not depend on the number of QDs in the chain. An increase in the standard deviation σ_X of QD centres from the prescribed values leads to a decrease in contrast, which is approximately the same for chains of different lengths (Fig. 11). The results obtained for a linear sensor structure indicate a monotonic decrease in contrast with increasing N, which is associated with a gradual decrease in the influence of an electron in the measured QD on nearby QD chains, and hence on photon transport through the MC. The consequence of this is the restoration of the polariton spectrum of the chain. In this case, the role of the Coulomb effects inside the chain is also levelled against the background of an increase in the electron-photon interaction.

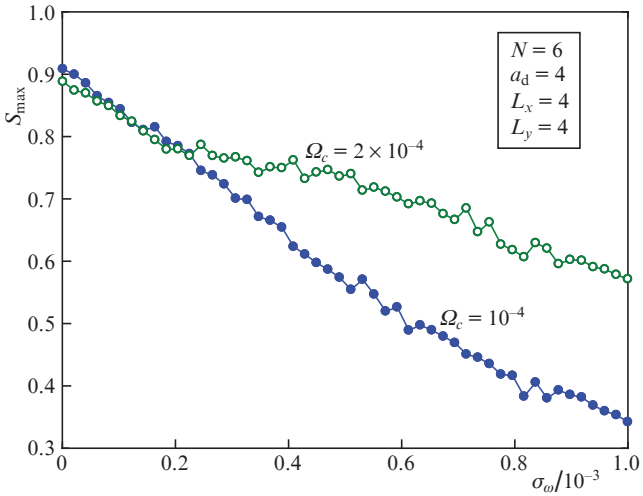

Figure 10. (Colour online) Dependences of the measurement contrast on the root-mean-square deviation of the QD transition frequency on the MC frequency. Each point is obtained by averaging over 1000 samples of random variables for each QD chain.

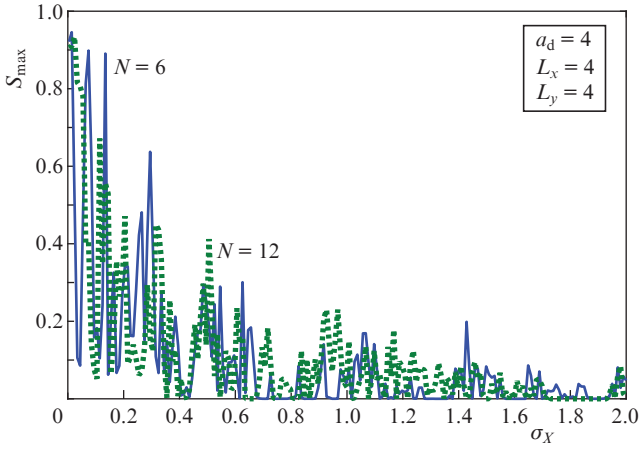

Figure 11. (Colour online) Dependences of the measurement contrast on the standard deviation of the QD coordinate for a short chain and a long one. Each point is obtained by averaging over 1000 samples of random variables (normal distribution) for each QD chain.

5. Conclusions

We have discussed the possibility of using a linear array of semiconductor single-electron QDs located at the antinode of the mode of an MC based on a two-dimensional PC as a detector of an electron located in the outer QD. The coefficient of photon transmission through the MC and the measurement contrast are calculated taking into account the Coulomb effects in the energy exchange between the QD and

the MC mode depending on the array parameters and the location of the measured QD. As follows from the simulation results, the Coulomb effects can either increase or decrease the sensitivity of the array to the external field produced by the electron. In addition, the stability of the system response to fluctuations in the QD parameters caused by the imperfection of their manufacturing technology is studied. Critical values of deviations are indicated, above which the operation of the measuring device becomes inefficient. Note that the principle of charge detection proposed in this work allows the use of QD arrays of various shapes, e.g., in the form of a ring.

Using the numerical solution of Maxwell's equations by the finite-difference time-domain method, the eigenfrequencies and electromagnetic field distributions in a two-dimensional PC with various types of defects are calculated. The PC parameters are chosen such that the Rabi frequency of the energy exchange of the MC mode with each QD in an array consisting of both several elements and a large number of QDs is approximately the same. The possibility of increasing the size of the antinode region of the electromagnetic field of the PC mode with an L-type defect is shown if it is necessary to use QD arrays consisting of several tens of elements.

The considered system has common features with an array of neutral atoms placed in an optical resonator [25]. However, there is also a significant difference because the structure of one-electron QDs is a charged system, while the collective of neutral atoms is not. This property brings the QD array closer to a chain of ions in a trap with a common phonon mode [26], as well as to a set of superconducting Josephson qubits in a coplanar microwave resonator [27]. All of them are characterised by high interaction energy and can be effectively controlled by external electromagnetic fields. In addition, an important advantage of schemes and networks based on QD in comparison with atomic schemes is their feasibility using existing planar lithographic technologies of micro- and nanoelectronics.

Acknowledgements. The investigation was supported by Program No. FFNN-2022-0016 of the Ministry of Science and Higher Education of Russia for Valiev Institute of Physics and Technology of RAS.

References

1. Joyce B.A., Kelires P.C., Naumovets A.G., Vvedensky D.D. *Quantum Dots: Fundamentals, Applications, and Frontiers* (NATO Science Series) (Dordrecht: Springer, 2003).
2. Michler P. *Single Semiconductor Quantum Dots* (Berlin: Springer, 2009).
3. Kouwenhoven L.P., Austing D.G., Tarucha S. *Rep. Progr. Phys.*, **64**, 701 (2001).
4. Barthel C., Kjærgaard M., Medford J., Stopa M., Marcus C.M., Hanson M.P., Gossard A.C. *Phys. Rev. B*, **81**, 161308(R) (2010).
5. Simmons C.B., Thalakulam M., Shaji N., Klein L.J., Qin H., Blick R.H., Savage D.E., Lagally M.G., Coppersmith S.N., Eriksson M.A. *Appl. Phys. Lett.*, **91**, 213103 (2007).
6. Ono Y., Fujiwara A., Nishiguchi K., Inokawa H., Takahashi Y. *J. Appl. Phys.*, **97**, 031101 (2005).
7. Gao M., Wang J., Fang S., Nan J., Daming L. *Int. J. Theor. Phys.*, **60**, 2358 (2021).
8. Tsukanov A.V., Kateev I.Yu. *Russ. Microelectron.*, **43** (5), 315 (2014) [*Mikroelektron.*, **43**, 323 (2014)].
9. Tsukanov A.V., Kateev I.Yu. *Russ. Microelectron.*, **43** (6), 377 (2014) [*Mikroelektron.*, **43**, 403 (2014)].
10. Tsukanov A.V., Kateev I.Yu. *Russ. Microelectron.*, **44** (2), 61 (2015) [*Mikroelektron.*, **44**, 79 (2015)]
11. Barenco A., Deutsch D., Ekert A., Jozsa R. *Phys. Rev. Lett.*, **74**, 4083 (1995).
12. Tsukanov A.V., Kateev I.Yu. *Russ. Microelectron.*, **42** (4), 197 (2013) [*Mikroelektron.*, **42**, 246 (2013].
13. Golovinskii P.A. *Semiconductors*, **48** (6), 760 (2014) [*Fiz. Tekh. Poluprovodn.*, **48**, 781 (2014)].
14. Tsukanov A.V. *Quantum Electron.*, **51**, 718 (2021) [*Kvantovaya Elektron.*, **51**, 718 (2021)].
15. Hennessy K., Badolato A., Winger M., Gerace D., Atatüre M., Gulde S., Fält S., Hu E. L., Imamoğlu A. *Nature*, **445**, 896 (2007).
16. Fink J.M., Bianchetti R., Baur M., Göppl M., Steffen L., Filipp S., Leek P.J., Blais A., Wallraff A. *Phys. Rev. Lett.*, **103**, 083601 (2009).
17. Aharonovich I., Niu N., Rol F., Russell K.J., Woolf A., El-Ella H.A.R., Kappers M.J., Oliver R.A., Hu E.L. *Appl. Phys. Lett.*, **99**, 111111 (2011).
18. Ding F., Stöferle T., Mai L., Knoll A., Mahrt R.F. *Phys. Rev. B*, **87**, 161116(R) (2013).
19. Moon S.-K., Jeong K.-Y., Noh H., Yang J.-K. *Appl. Phys. Lett.*, **109**, 241106 (2016).
20. Kuruma K., Ota Y., Kakuda M., Takamiya D., Iwamoto S., Arakawa Y. *Appl. Phys. Lett.*, **109**, 071110 (2016).
21. Hennessy K., Reese C., Badolato A., Wang C.F., Imamoğlu A., Petroff P.M., Hua E., Jin G., Shi S., Prather D.W. *Appl. Phys. Lett.*, **83**, 3650 (2003).
22. Jarlov C., Wodey É., Lyasota A., Calic M., Gallo P., Dwir B., Rudra A., Kapon E. *Phys. Rev. Lett.*, **117**, 076801 (2016).
23. Hagemeier J., Bonato C., Truong T.-A., Kim H., Beirne G.J., Bakker M., van Exter M.P., Luo Y., Petroff P., Bouwmeester D. *Opt. Express*, **20**, 24714 (2012).
24. Badel M., Wiersig J. *Phys. Rev. A*, **99**, 063825 (2019).
25. Ritsch H., Domokos P., Brennecke F., Esslinger T. *Rev. Mod. Phys.*, **85**, 553 (2013).
26. Bruzewicz C.D., Chiaverini J., McConnell R., Sage J.M. *Appl. Phys. Rev.*, **6**, 021314 (2019).
27. Kwon S., Tomonaga A., Bhai G.L., Devitt S.J., Tsai J.-S. *J. Appl. Phys.*, **129**, 041102 (2021).